Acta Geologica Sinica (English Edition), 2022, 96(5): 1716–1728

Ambient Noise Tomography of Jinan: The Migration of Groundwater and the Formation of Geothermal Water

LEI Ting[1, 2, 3], LIANG Feng[1, 2, *], HAN Chen[1, 2, 4], WANG Zhihui[1, 2], LI Junlun[3, 5], MA Yan[1, 2] and YAO Huajian[3, 5]

[1] *Chinese Academy of Geological Sciences, Beijing 100037, China*
[2] *SinoProbe Center, Chinese Academy of Geological Sciences and China Geological Survey, Beijing 100037, China*
[3] *Laboratory of Seismology and Physics of the Earth's Interior, School of Earth and Space Sciences, University of Science and Technology of China, Hefei 230026, China*
[4] *China University of Geosciences (Beijing), School of Geophysics and information technology, Beijing 100083, China*
[5] *National Geophysical Observatory at Mengcheng, University of Science and Technology of China, Mengcheng, Anhui 233500, China*

Abstract: Jinan is an important city in eastern China, with rich groundwater in the region. There are four famous springs in the urban area and an abundance of geothermal water in the northern part, which makes the migration of groundwater in this area a very important issue. To study the shallow shear wave velocity structure and groundwater migration in Jinan, we utilized almost a month of continuous waveform data from 175 short period seismometers deployed by the Chinese Academy of Geological Sciences, in order to calculate the cross-correlation function. We picked 7749 group dispersion curves and 6117 phase dispersion curves with a period range of 0.2–2 s. Through inversion, we obtained the fine three-dimensional shear wave velocity and azimuthal anisotropy structure (0–2.4 km). Combining the results with local geological and hydrological data, the following conclusions were reached. (1) There are widespread high velocity anomalies in the region between the Qianfoshan and Wenhuaqiao faults, as well as to the east of the Wenhuaqiao Fault, which may be related to the intrusive gabbro known as the Jinan Intrusive Rock. (2) The two distinct high velocity anomalies in our model (referred to as west and east Jinan Intrusive Rock in this paper) may indicate that the Jinan Intrusive Rock was broken through crustal movement. (3) There is an obvious low velocity layer under the intrusive rock, which could be the channel of groundwater migration. The precipitation in the southern mountain region seeps down into the ground, then is blocked by the Jinan Intrusive Rock and can only progress downwards to a deeper part, where the groundwater is heated by the geothermal gradient. The heated water finally arrives at the northern part and forms geothermal water. (4) The depth of the low velocity layer beneath the Jinan Intrusive Rock varies laterally, which may indicate that the depth of the groundwater migration is different beneath the west and east Jinan Intrusive Rock. (5) There is strong azimuthal anisotropy in southern Jinan, with nearly E-W fast orientation, which may be related to the tilt limestone layering structure.

Key words: ambient noise tomography, shear wave velocity structure, urban underground space, Jinan groundwater, Baotu Spring Park

Citation: Lei et al., 2022. Ambient Noise Tomography of Jinan: The Migration of Groundwater and The Formation of Geothermal Water. Acta Geologica Sinica (English Edition), 96(5): 1716–1728. DOI: 10.1111/1755-6724.14808

1 Introduction

Jinan is located in midwestern Shandong province, eastern China. As one of the most important cities of the Bohai Rim region and the lower reaches of the Yellow River, it is the provincial capital of Shandong, with a permanent population of more than 7 million. Jinan sits on the southeast edge of the North China Plain, on the northern edge of the central Shandong mountains, south of the Yellow River and north of the Taishan Mountain. The terrain is high in the south and low in the north: the altitude of the southern mountainous area is about 100–500 m, the altitude of the central tilted plain is about 20–100 m and the altitude on the northern alluvial plain in the middle and lower reaches of the Yellow River is below 20 m.

Jinan is famous as the Spring City, with many famous springs being located in the urban region. On the one hand, these springs are important scenic spots and attract many tourists, but on the other, these springs are also disruptive factors in city construction (Zhang et al., 2017). Springs are associated with abundant groundwater and in Jinan, the groundwater has caused some troubles in the construction of underground transportation (Yang et al., 2012; Wang et al., 2018a). In recent years, the spring flow has declined a lot. Geological modelling has provided some suggestions for spring protection (Wu and Xu, 2005; Qian et al., 2006; Kang et al., 2011).

In addition to spring water, the groundwater also exists in another form, that of geothermal water. There are plenty

* Corresponding author. E-mail: imr_liangfeng@cags.ac.cn

of geothermal wells around Jinan (Feng et al., 2013), especially in the north. Gao et al. (2009) divided the geothermal resources in this region into three categories (Fig. 1): (A) Paleozoic karst-crack geothermal water in the mountain area of central Shandong; (B) Paleozoic karst-crack geothermal water in the depression area of west Shandong; (C) Cainozoic pore-crack geothermal water in the depression area of northwestern Shandong. Categories A and B are stored in the plain area and are referred to as the Geothermal Field in Northern Jinan.

The formation of geothermal water in north Jinan is an important question in this region for the reasonable utilization of the geothermal resource. The proportion of light and heavy isotopes can be affected by evaporation and liquefaction. The oxygen and hydrogen isotope characteristics of the geothermal water are similar to that of precipitation, which means that the geothermal water is likely to be supplied by the precipitation from the southern mountain region (Li et al., 2008; Wang et al., 2016). The cold water from the southern part seeps down to a deeper part, where it is heated by a deep loop (Liang, 2012).

The infiltration of precipitation is related to the famous intrusive rocks beneath the Jinan urban district. The intrusive event happened in the Early Cretaceous, according to isotopic dating studies (Xu W L et al., 2004; Xu Y G et al., 2004; Yang et al., 2005). The intrusive rocks are composed of klinaugite, anorthose and amphibole etc. The rocks came from the lithospheric mantle and were contaminated by lower crustal material (Gao and Chen, 2013; Ding et al., 2016).

As it has been a long time since the intrusive event, the heat carried by the intrusive rocks has been lost. The geothermal gradient in this region is about 3.66°C/100m, the water being heated by intrinsic geothermy because it reaches a depth of about 2 km (Liang, 2012). The water migration model is also supported by the close connection of the southern cold water and the northern geothermal water. The water level in the two regions is highly correlated (Zhao et al., 2009). The gradual change of the ionic composition in the water from south to north can be explained by this model (Sui et al., 2017; Cheng, 2018; Cheng et al., 2019).

In summary, petrological and hydrochemical studies have depicted the general relationships of the intrusive rocks and water migration, but the location of the water migration tunnel remains undiscovered. In this study, we use ambient noise tomography to invert for the shear wave velocity model and anisotropy model beneath Jinan. Combined with local geological data, our model provides a different perspective from which to understand the water migration tunnel in this area. The safety of cities is becoming more important with their development. Studying a city's underground space using ambient noise data from a dense array can easily be applied to other cities, in order to establish a database for earthquake prevention and disaster reduction.

2 Methods and Data

Ambient noise tomography has been widely used to

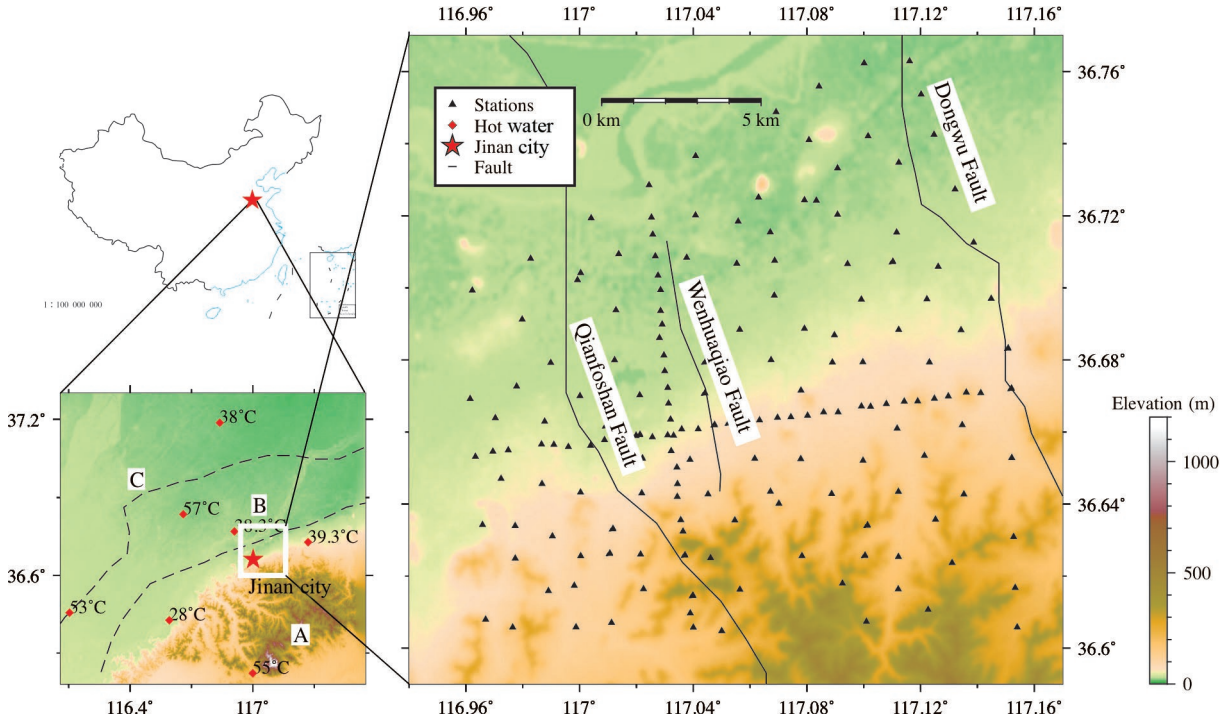

Fig. 1. Geological background of the study area and distribution of stations.

The red star represents the location of Jinan City. The dashed lines are the boundaries between different geothermal water types: (A) Paleozoic karst-crack geothermal water in the mountain area of central Shandong; (B) Paleozoic karst-crack geothermal water in the depression area of western Shandong; (C) Cainozoic pore-crack geothermal water in the depression area of northwestern Shandong. The red diamonds are locations of geothermal water, with the corresponding texts indicating the average temperatures. The black triangles are the stations. The black lines are three faults in the region. China basemap after China National Bureau of Surveying and Mapping Geographical Information (No: GS (2019) 1652).

build regional or global shear wave velocity models. Recently, this method has been applied to study the structure beneath cities (Li et al., 2016; Liang et al., 2018, 2019a, b). The advantages of this method are: (1) it does not rely on earthquake data, so is applicable to regions lacking seismic activity, such as Jinan; (2) compared with active source methods, it is cheaper and easier to implement (Liu et al., 2015); (3) the shear wave velocity revealed by ambient noise tomography is especially sensitive to water, so it is highly suitable for use in studying the water migration in Jinan.

However, the city region is noisy and full of local ambient noise sources. The noise of human activity can reduce the signal-to-noise ratio of the cross-correlation function. Additionally, the shallow structure is strongly heterogeneous, which increases the difficulty of selecting dispersion curves. These problems can be resolved by using a more reasonable process flow.

2.1 Data processing

175 short period seismometers were deployed in the urban region of Jinan with an average spacing of about 1 km (Fig. 1). 27 days of continuous waveform were recorded. After data preprocessing (Bensen et al., 2010), the daily cross-correlation was calculated in 0.15–0.5 s and 0.5–2.0 s. Through linear stacking, the final cross-correlation functions were obtained. The surface wave signal in both 0.2–0.5 s and 0.5–2.0 s was clear (Fig. 2).

Dispersion curves were then selected, based on the image analysis method (Yao et al., 2018). Considering the strong heterogeneity in short periods, group velocity dispersions were the first selected. The group velocity dispersion curves are easier to select but the measuring error is larger, while the phase velocity dispersions are more accurate and difficult to pick. In this study, a reference model was built using group velocity dispersions, the phase velocity dispersions then being selected, based on this reference model. This procedure can reduce the chance of selecting the wrong phase velocity dispersion branches. Cluster analysis was also used to increase the reliability of the dispersion curves (Zhang et al., 2018). Finally 7749 group velocity dispersion curves and 6117 phase velocity dispersion curves were obtained (Fig. 3). The ray paths cover the

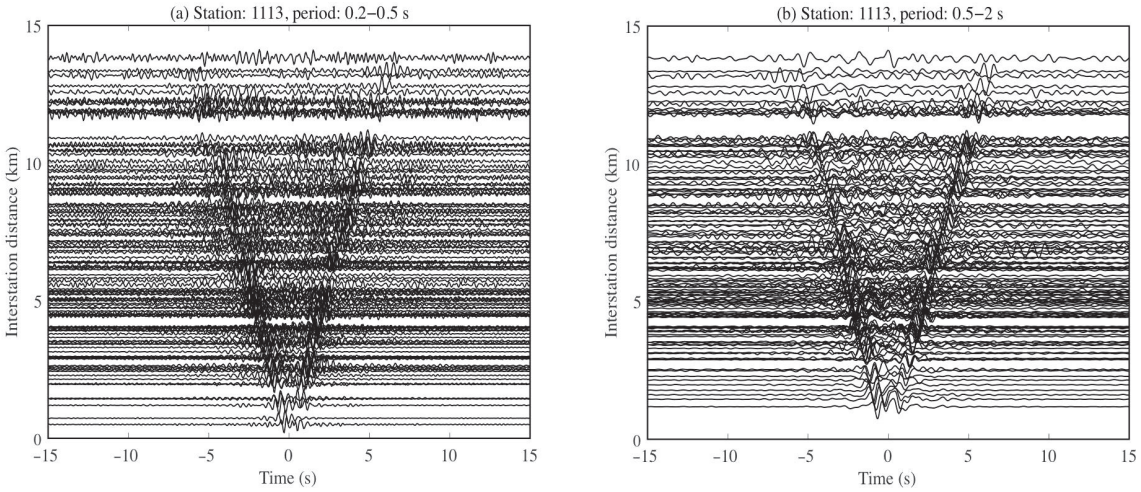

Fig. 2. Cross-correlation function of station 1113 with other stations in the shorter (0.2–0.5 s) and longer (0.5–2 s) period band.

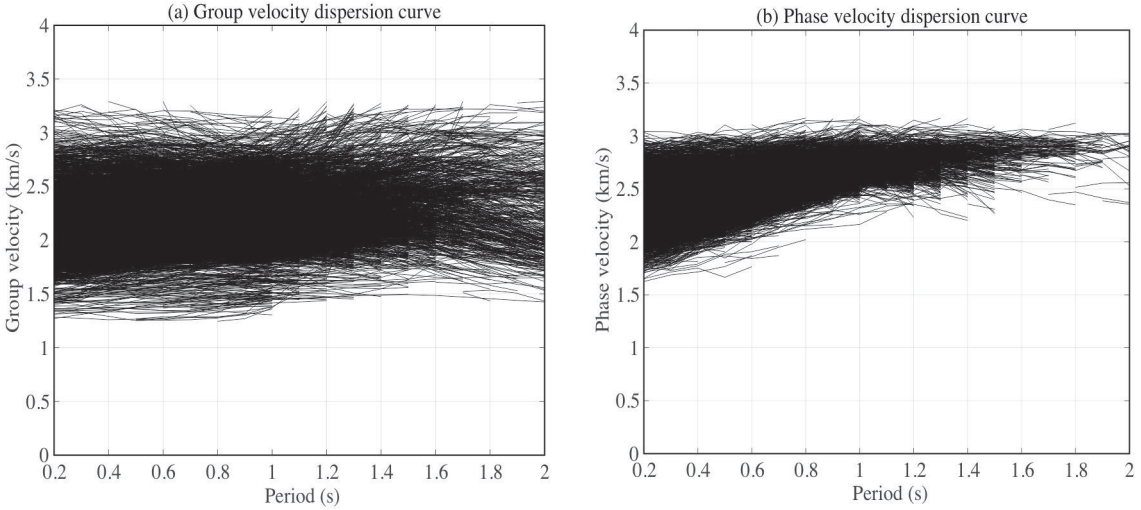

Fig. 3. Group and phase velocity dispersion curves.

study region very well and were counted on 0.01° × 0.01° grids in each period. In the central part, the number of paths in a single grid was over 1000 (Fig. 4). In the inversion, the data of 0.2 s to 2 s with 0.1 s interval was used. The short periods were covered with more abundant ray paths. Even in long periods, there were about 1000 ray paths in one period (Fig. 5).

2.2 Inversion method

The direct inversion method proposed by Fang et al. (2015) was used to do the inversion. Differing from the traditional two-step method, which inverts for the 2D phase/group velocity map prior to obtaining the shear velocity model, the direct inversion method can obtain the shear velocity model directly from the phase/group velocity dispersion measurements. Another important difference is that the direct inversion method uses the ray tracing path rather than thegreat circle path, as when the study region is laterally heterogeneous, the ray paths will bend and be far away from the great circle path. According to the local geological setting, there are some intrusive rocks in the study area, so the direct inversion method can be helpful to simulate the bending ray paths.

The inversion grid was 0.01° × 0.01° in the horizontal direction. In the vertical direction, the maximum depth was 5.2 km and the grid interval was not uniform. The grid point interval was 0.1 km from 0.1 km to 0.8 km and it was 0.2 km from 0.9 km to 1.5 km. The interval increases with increasing depth, until the deeper part cannot be resolved anymore. The dense grids in the shallow part can parameterize the velocity structure more accurately and the sparse grids in the deeper part can absorb the residual of longer periods. The direct inversion method requires a damping parameter to balance the residual and the smoothness of the model. A series of damping values were tested and L-curves plotted, in order to choose a proper parameter, ultimately conducting the inversion with a damping of $\lambda = 50$.

After deriving the isotropy model, the anisotropy parameters were added to obtain the azimuthal anisotropy structure of Jinan. The inversion was carried out using the package developed by Liu et al. (2019). As this package is

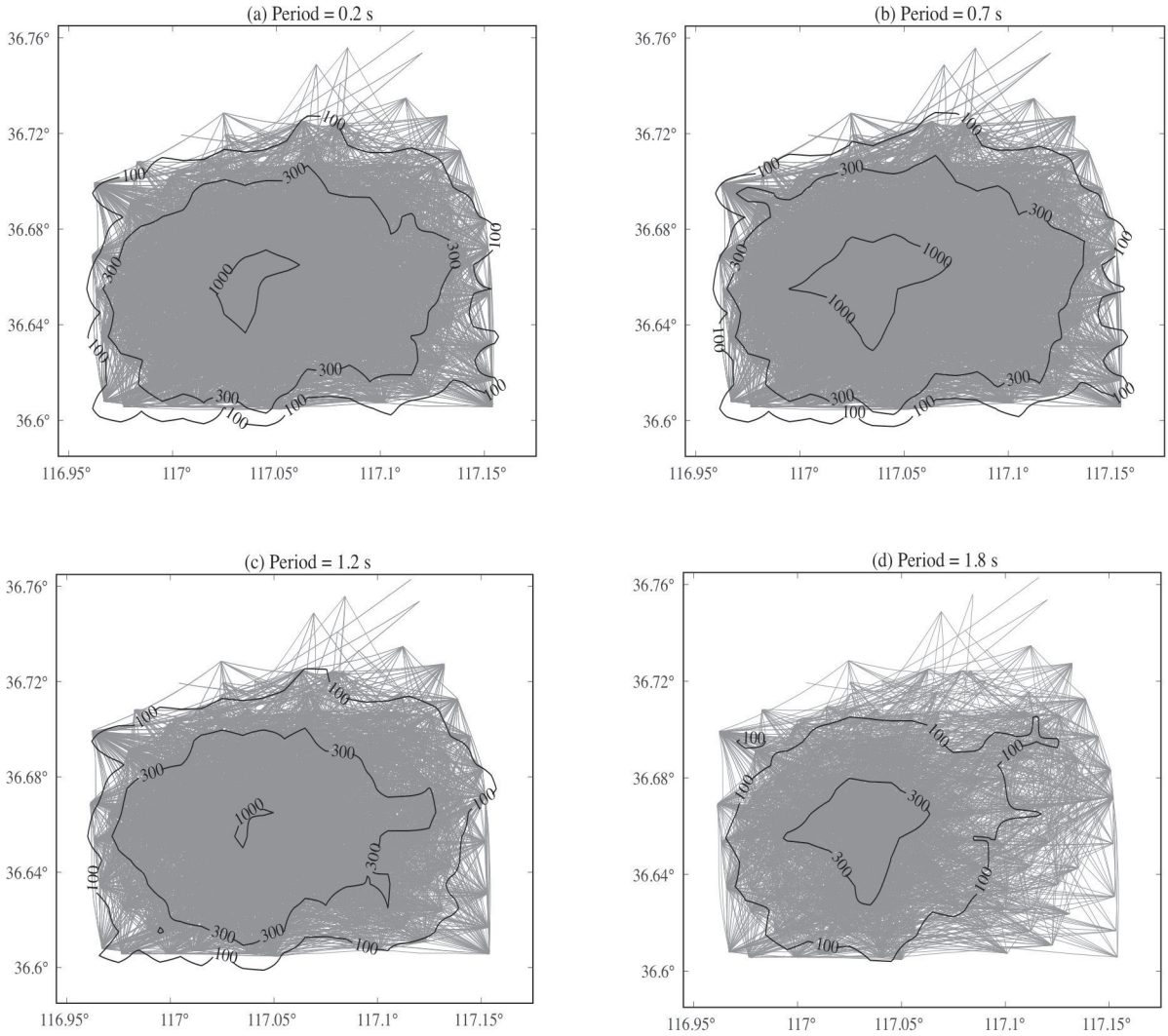

Fig. 4. Ray coverage in different periods.
The gray lines are the ray path and the black contours denote the number of ray paths in a 0.01° × 0.01° grid point.

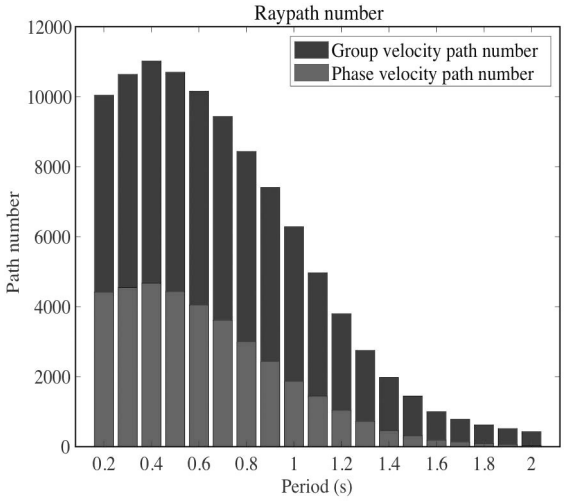

Fig. 5. The number of group velocity and phase velocity measurements in different periods.
The blue part denotes the amount of group velocity paths and the red part denotes the amount of phase velocity paths.

based on the framework of the direct inversion method, the ray path bending is also properly simulated. With the joint inversion of isotropic and anisotropic structure, the trade-off between heterogeneity and anisotropy can be mitigated. In the anisotropic inversion, only the phase velocity dispersion was used.

3 Results

3.1 Isotropic model

The depth sensitivity kernel of phase and group velocity dispersion was calculated before the inversion of the real data. The group velocity dispersion data of 0.7 s was sensitive to the structure of around 0.5 km and the phase velocity dispersion data of 1.8 s was sensitive to the structure of around 2 km (Fig. 6). In the same period, the sensitive depth of phase velocity dispersion is slightly larger than that of group velocity dispersion. In total, the data can resolve the structure of 0–2 km.

The checkerboard resolution test was also performed to evaluate the lateral resolution. The checkerboard model was built by adding ±5% velocity anomalies to adjacent

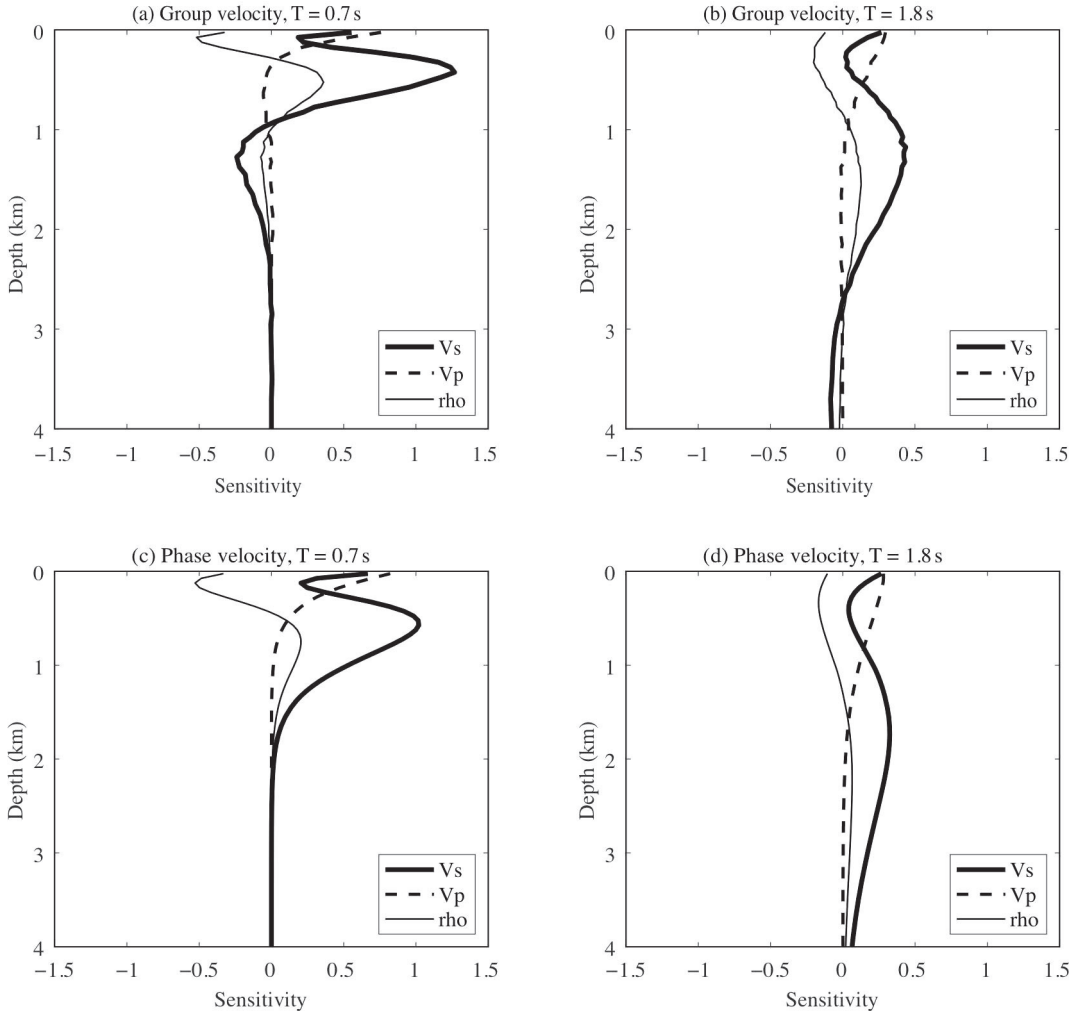

Fig. 6. Sensitivity kernel of group and phase velocity dispersion in different periods.
The bold lines denote sensitivity to shear wave velocity, the thin lines denote the sensitivity to compression wave velocity, the dashed lines denote the sensitivity to density.

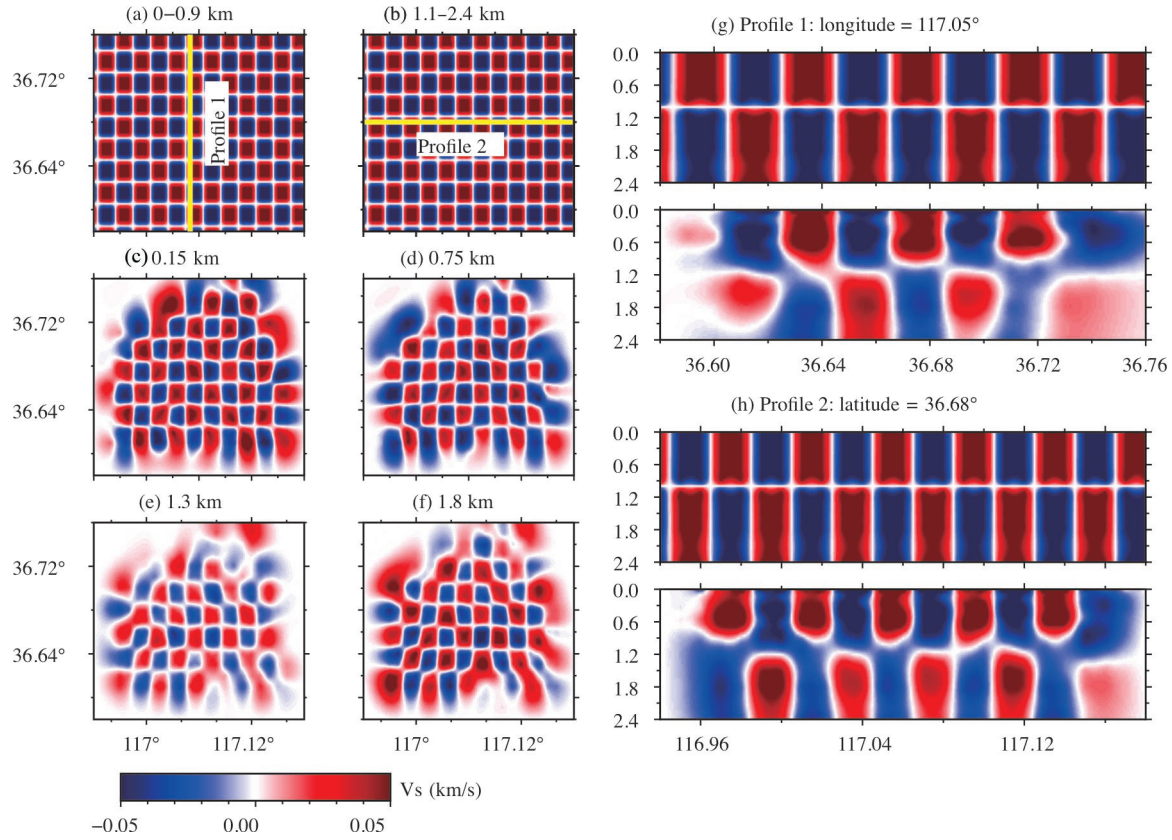

Fig. 7. Checkerboard test: (a–f) are horizontal slices.
(a–b) are the settings of the target model; (c–f) are the recovered slices at different depths; (g–h) are vertical slices. The location of two slices are marked with a yellow line in (a) and (b). The upper two show the true model while the lower two show the recovered model.

grid points (0.02° × 0.02°, about 2 km) based on the 1-D velocity model. The 1-D model was built from the inversion with the average dispersion curve. The anomaly below 1 km is contrary to the anomaly above 1 km. 1% Gaussian noise was added to the theoretical dispersions calculated from the true model. After the inversion, the structure of 0–2.4 km could be recovered. With the abundance of phase and group velocity dispersion, the shallow structure could be resolved well.

The fine shear wave velocity model of shallow Jinan (Fig. 8) was obtained from the inversion of the real data. There is a strong shear wave velocity contrast between the south and the north. The low velocity zone is widespread in the south, while the high velocity anomalies are distributed in the north. The high velocity anomaly is separated, the boundary being the Wenhuaqiao Fault. From the vertical slice (Fig. 10), a low velocity layer is apparent beneath the high velocity anomalies.

3.2 Anisotropic model

The anisotropic checkerboard is carried out (Fig. 9). The anisotropy anomaly pattern is 0.04° and the amplitude is 3%. The fast orientation of the true model are 0° and 90°. When the test is noise-free, both the anisotropy anomalies in the shallow part and the deeper part are recovered. When there is 1% Gaussian noise, only the anisotropy of the shallow part can be resolved.

The anisotropic model of shallow Jinan was obtained. Southern Jinan has strong azimuthal anisotropy, while the anisotropy in the north is weaker. In the south, the anisotropy magnitude can reach 5%. The fast orientation in the E-W is east-west and it is NEE-SWW in the northeast.

4 Discussion

4.1 Intrusive rocks and fault activity

There are widespread intrusive rocks in Jinan. The high velocity anomalies in the northern part may be related to the Jinan Intrusive Rock. Geological studies have clarified the source and age of these rocks (Yang et al., 2005; Gao and Chen, 2013; Ding et al., 2016), while the spatial distribution of these rocks is still not clear. In this study, the Jinan Intrusive Rock is clearly shown by the high velocity anomaly. Magma tunnels are necessary for intrusions. In the model, the high velocity anomaly in the deeper part is distributed in the northwest, which may indicate that the intrusion was from the northwest of Jinan.

The Jinan Intrusive Rock is broken into two parts, referred to here as west and east Jinan Intrusive Rock (Fig. 10). The break-up of the rock may have been caused by fault activity, there being three faults in the study area (Qianfoshan Fault, Wenhuaqiao Fault and Dongwu Fault), which are all normal faults. The Qianfoshan Fault is about 30 km long and is the biggest fault in the region (Liu,

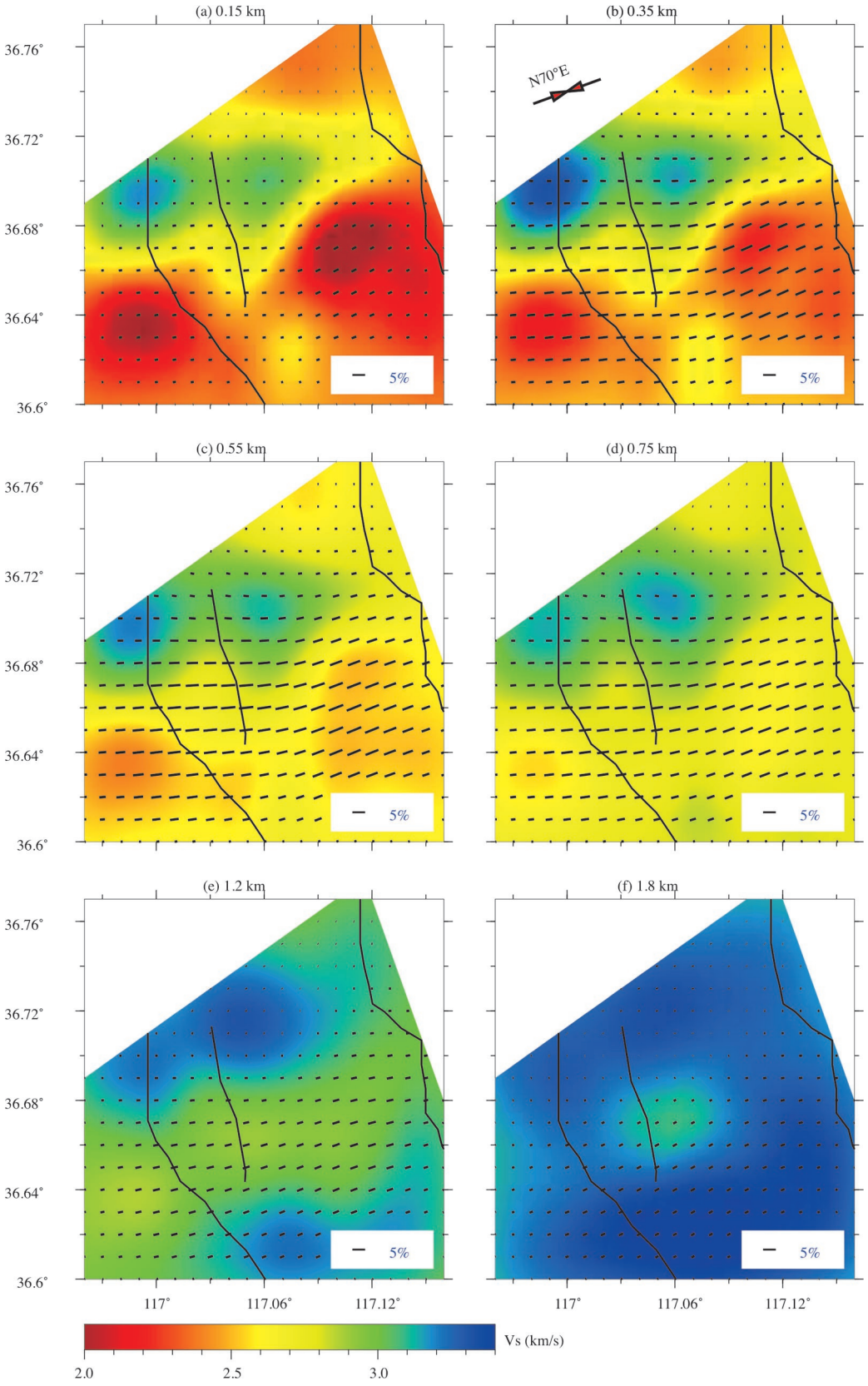

Fig. 8. Horizontal slices of the model at different depths.
The short bars are the fast wave directions. The black lines are faults. The arrow in (b) shows the maximum principal compressive stress direction of the nearby area (Feng et al., 2017). The average direction in this region is a good reference of the local stress field, because the stress field of this region is relatively stable (Feng et al., 2017).

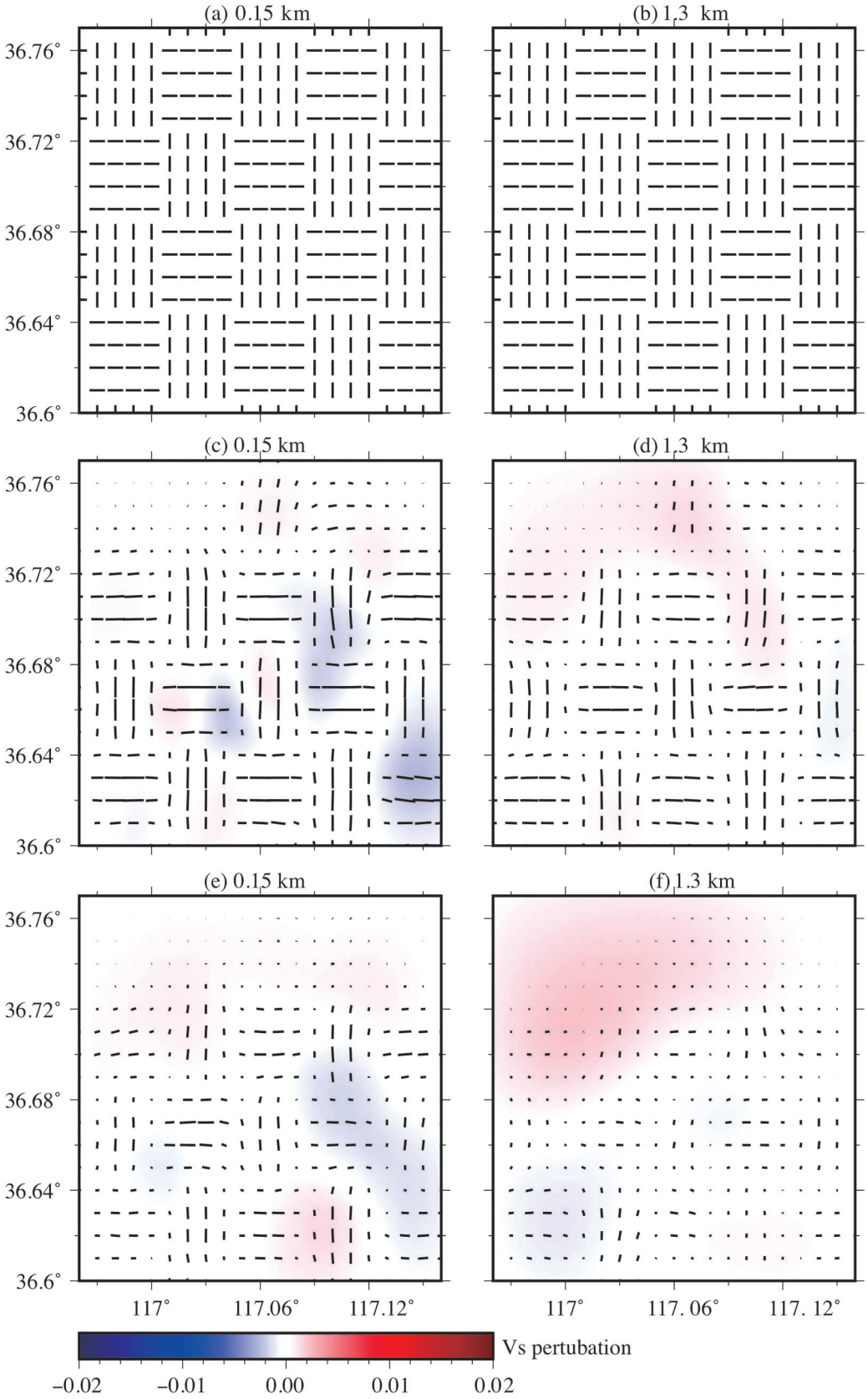

Fig. 9. Azimuthal anisotropy checkerboard.
(a–b) are the true model; (c–d) are the inversion model produced by using noise-free synthetic data; (e–f) are the inversion model produced by using data with 1% Gaussian noise. The background of (c–f) is the isotropic perturbation of the anisotropic inversion.

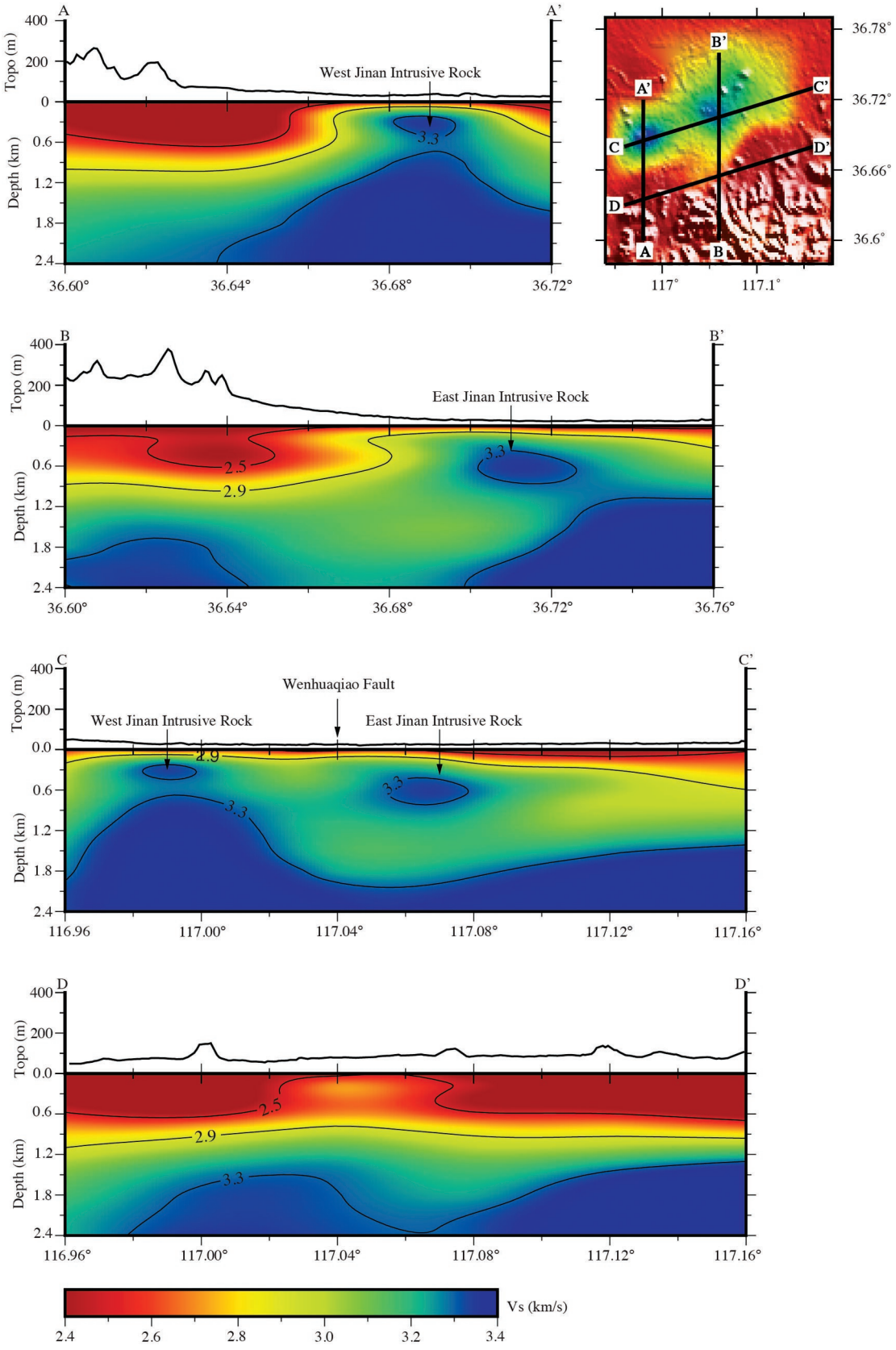

Fig. 10. Vertical slices in the study region.
The location of the profiles is shown in the upper right figure.

2009; Song et al., 2016). The Wenhuaqiao Fault is a small one and it is only 3–4 km long, however, the break-up of the Jinan Intrusive Rock may be related to the Wenhuaqiao Fault, as the Qianfoshan Fault has no clear velocity change.

The formation of the low velocity belt between the two high velocity anomalies is quite clear. The fracture zone of the fault can be filled by air and water, so the shear wave velocity of the fracture zone can obviously be reduced. Groundwater in Jinan is abundant, the deeper part of the Wenhuaqiao Fault being water conductive (Wang et al., 2018b). The low velocity belt may come from groundwater activity in the Wenhuaqiao Fault. Qianfoshan Fault does not affect the shear wave velocity around it and this requires more research to be conducted, regarding the structure of this fault.

4.2 Origin of the azimuthal anisotropy

The azimuthal anisotropy is strongly linked to regional evolutionary history. In the study area, there is clearly approximately E–W azimuthal anisotropy. Combined with local geological structural knowledge, there are two possible origins of the azimuthal anisotropy, specifically limestone layering and regional stress.

Unlike the high velocity in the northern region, southern Jinan has low velocity. This area is full of limestone, which has a lower shear wave velocity and is often layered. When the wave propagates through a layered medium, the velocity along the bedding plane is higher while the velocity perpendicular to the bedding plane is lower. When the layered medium is inclined, the velocity along the strike is higher and the velocity along the dip is lower (Grechka et al., 2001; Wang, 2002). When the northern mountain region was uplifted, the limestone became north-dipping. This can lead to E-W fast orientation.

The azimuthal anisotropy is also related to the regional stress field. When the medium is under compressive stress, cracks perpendicular to the compressive stress will close. The principle compressive stress direction will be the fast axis direction. Previous studies about the stress field around Jinan revealed that the principal compressive stress was NEE–SWW (Miao et al., 2009; Feng et al., 2017), which is also consistent with these results.

The azimuthal anisotropic magnitude in the southern region is noted as strong and the fast axis directions of the two low velocity blocks are slightly different. The fast orientation of the southwest is E–W, while that of the southeast is NEE–SWW. Different fast orientations may reveal a slightly different dip direction between the two limestone blocks. The southwestern limestone block is strictly north-dipping, while the southeastern one is not. As shown by the fast orientation change in the south, the limestone layering may be the main reason underlying the azimuthal anisotropy. However, the northern part, which is not layered, also has weak anisotropy, so the regional stress may also contribute to the azimuthal anisotropy.

In summary, the azimuthal anisotropy in the study area may be affected by both layered limestone and regional stress field. The regional stress has a widespread but weaker effect. The layered limestone is the main reason for the southern strong anisotropy.

4.3 Groundwater migration and the formation of geothermal water

The distribution of water is an important question in Jinan. The hydrochemical study revealed the connection of the northern geothermal water and the southern cold water. In the results from the tomography, the low velocity layer beneath the intrusive rock might represent the water migration tunnel.

The depth resolution of ambient noise tomography is limited, due to the smooth surface wave sensitivity kernel, so model recovery test was performed to check if a low velocity layer could be resolved (Fig. 11). The background model is the 1-D model inverted from average dispersion. The two high velocity anomalies were added to simulate the distribution of the intrusive rock. The initial model is

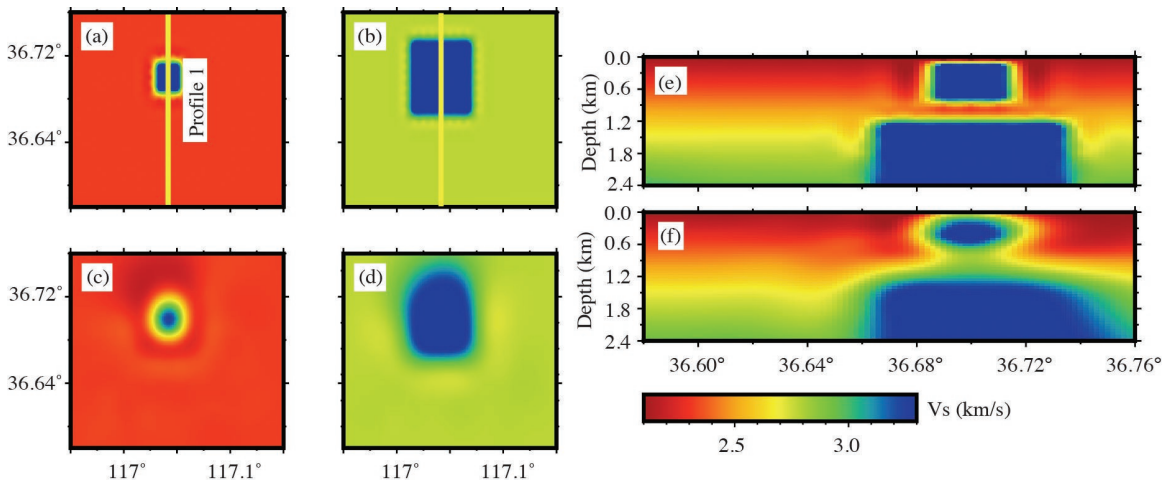

Fig. 11. Model recovery test.
(a–b) are the setting of the true model at depths of 0.55 km and 1.8 km; (c–d) are the recovered model at depths of 0.55 km and 1.8 km; (e) the setting of the true model beneath profile 1 (the location is marked in (a)); (f) the recovered model beneath Profile 1.

the simple 1-D model. With 1% Gaussian noise, the high velocity anomalies and the low velocity layer are clearly recovered. The low velocity layer in the results is therefore relatively reliable.

The formation of the northern geothermal water is through a deep loop, so the maximum depth of the deep loop is very important. According to the local geothermal gradient, the maximum depth of the deep loop was estimated to be about 2 km (Zhao et al., 2009), which is consistent with the results in this study. The depth of the deep loop varies in different regions, being capable of reaching 2 km beneath the east Jinan Intrusive Rock, but the water migration tunnel only lies at about 0.6 km depth beneath the west Jinan Intrusive Rock.

Blocked by the Jinan Intrusive Rock, the precipitation in the south goes down to a deeper area. It is assumed that there is a weakened root beneath the Jinan Intrusive rock, as supported by two points. (1) The intrusive rock is basic, so it is relatively easily eroded. Furthermore, given that the water is heated, the erosion process may well be accelerated. (2) The variation of ions from south to north also supports the breakdown of basic rocks (Cheng, 2018; Cheng et al., 2019). The increase of Cl^- in the water from the south to the north can be explained by the erosion of rocks such as hornblende (Sui et al., 2017). Overall, the weakening of the root is more or less clear, although the degree to which it is weakened is difficult to determine. More quantitative work needs to be done to investigate the interaction of heated water and intrusive rocks.

4.4 Water migration model beneath Jinan

In conclusion, the shear wave velocity model produced reveals the following characteristics about Jinan: (1) the north-dipping limestone layering is revealed by the nearly E–W fast orientation; (2) the intrusive rock is indicated by the high velocity anomalies in the north; (3) the groundwater migration tunnel is shown by the low velocity layer beneath the Jinan Intrusive Rock. With this model, the geological structure is better understood. A more delicate groundwater migration model was built in Jinan (Fig. 10B–B'; Fig. 12).

The precipitation in the southern mountain region flows to Jinan as a result of the topography. In the shallow part, the water supplies the spring in Jinan. In the deeper part, the water is blocked by the Jinan Intrusive Rock and can only seep down to the deeper part. The karst caves and north-dipping limestone layering can help the start of the deep loop.

The water at greater depths is heated by the geothermal gradient. The root of the intrusive rocks is eroded and weakened by hot water. After the weakening of the root, the hot water can migrate to the north easily. Finally, the cap rocks in the northern part are heat-insulated (Shi et al., 2005), so the geothermal water can be preserved in this region.

5 Conclusions

Isotropic and anisotropic shear wave velocity models were obtained for the Jinan urban region from ambient noise tomography. In the north, the intrusive rocks were indicated by the high velocity anomaly. The Jinan Intrusive Rock is broken by the Wenhuaqiao Fault. In the south there is widespread limestone, which has a lower shear wave velocity.

The azimuthal anisotropy in this region is pronounced. The fast orientation is in an approximately E–W direction. The azimuthal anisotropy is mainly caused by the north-dipping limestone, so that the anisotropic magnitude is higher in the southern and lower in the northern intrusive rock region. Regional stress may also contribute to the anisotropic structure, but only to a minor degree.

The formation of geothermal water in this region is caused by the unique geological setting. The high mountains in the south, the north-dipping limestone and the block of the Jinan Intrusive Rock help the precipitation to seep down to deeper parts. The water may erode the root of intrusive rock so that the water can migrate to the north. The details of the interaction between the water and the intrusive rocks is unclear and requires more research.

Ambient noise tomography shows the shallow structures of Jinan. This shear wave velocity model can

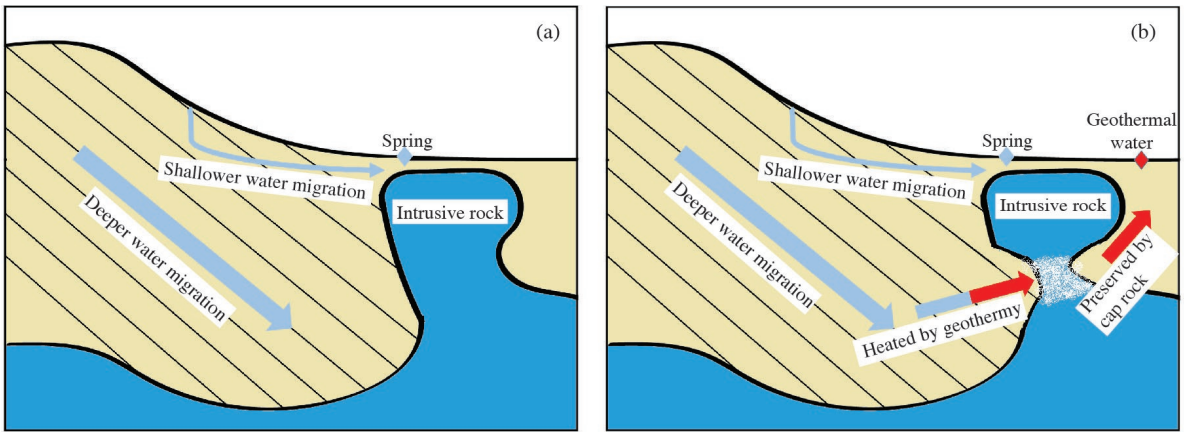

Fig. 12. (a) The precipitation seeps down to a deeper area; (b) the root of the Jinan Intrusive Rock is weakened by the heated water, the geothermal water can easily be transported to the northern part.

not only be the foundation of earthquake disaster assessment, but also the basis on which to do more refined work in this region. Exploring the shallow structure of the urban region using ambient noise tomography can be widely used in other cities for more reasonable utilization of urban underground space.

Acknowledgments

This study was funded by the Chinese Geological Survey Project (Grant No. DD20211314), basic scientific research project from the Chinese Academy of Geological Sciences (Grant Nos. YWF201901-02), the National Key Research and Development Program of China 'Technology helps economy' 2020 Project (Grant No. SQ2020YFF0426563).

Manuscript received Jun. 7, 2021
accepted Sep. 15, 2021
associate EIC: XU Tianfu
edited by Jeffery J. LISTON and FANG Xiang

Reference

Bensen, G.D., Ritzwoller, M.H., Barmin, M.P., Levshin, A.L., Lin, F., Moschetti, M.P., Shapiro, N.M., and Yang, Y., 2010. Processing seismic ambient noise data to obtain reliable broad -band surface wave dispersion measurements. Geophysical Journal of the Royal Astronomical Society, 169(3): 1239–1260.

Cheng, H.Z., 2018. Probing into geothermal resource features, exploitation and utilization in the Ningjiabu area to the east of Jinan. Coal Geology of China, 30(S1): 76–79.

Cheng, H.Z., Cheng, S.C., and Wang, Z.T., 2019. Study on hydrogeochemical evolution mechanism of 'Ordovician Limestone' geothermal fluid based on hydrochemical characteristics–Setting No. 1 Zhangning geothermal well in eastern Jinan as an example. Shandong Land and Resources, 35(8): 20–25 (in Chinese with English abstract).

Ding, X.L., Ren, Z.Y., Guo, F., Qian, S.P., Zhang, L., Huang, X.L., Chen L.L., Zhang, Y.H., Hong, L.B., Zhang, Y., and Wu, Y.D., 2016. Magmatic processes involved in formation of the Jinan gabbro: evidence from melt inclusions. Geotectonica et Metallogenia, 40(01): 174–190.

Fang, H.J., Yao, H.J., Zhang H.J., Huang, Y.C., and van der Hilst, R.D., 2015. Direct inversion of surface wave dispersion for three-dimensional shallow crustal structure based on ray tracing: Methodology and application. Geophysical Journal International, 201: 1251–1263.

Feng, C.J., Zhang, P., Qi, B.S., Meng, J, Tan, C.X., and Hu, D.G., 2017. Recent tectonic stress field at the shallow Earth's crust near the Tan-Lu Fault zone. Geoscience, 31(1): 46–70.

Feng, S.T., Xu, Y., and Yang, X.C., 2013. Geothermal characters of deep karst thermal reserve in Shandong Province. Shandong Land and Resources, 29(09): 16–22+30 (in Chinese with English abstract).

Gao, L., and Chen, B., 2013. Study on petrology, geochemistry and Os-Nd-Sr isotopes of Jinan gabbro in Luxi Block. Journal of Earth Sciences and Environment, 35(2): 19–31 (in Chinese with English abstract).

Gao, Z.J., Wu, L.J., and Cao, H., 2009. The summarization of geothermal resources and its exploitation and utilization in Shandong Province. Journal of Shandong University of Science and Technology (Natural Science), 28(02): 1–7 (in Chinese with English abstract).

Grechka, V., Pech, A., Tsvankin, I., and Han, B., 2001. Velocity analysis for tilted transversely isotropic media: A physical modeling example. Geophysics, 66(3): 904–910.

Kang, F.X., Jin, M.G., and Qin, P.R., 2011. Sustainable yield of a karst aquifer system: A case study of Jinan springs in northern China. Hydrogeology Journal, 19(4): 851–863.

Li, C., Yao, H.J., Fang, H.J., Huang, X.L., Wan, K.S., Zhang, H.J., and Wang, K.D., 2016. 3D Near-surface shear-wave velocity structure from ambient-noise tomography and borehole data in the Hefei urban area, China. Seismological Research Letters, 87(4): 882–892.

Li, C.S., Yang, L., Gao, W.X., and Wang S.J., 2008. Analysis on geological characteristics of geothermal field in north part of Jinan City. Shandong Land and Resources(04): 35–39.

Liang, Y., 2012. Geothermal exploration and development in the north of Jinan. Geology and Chemical Minerals, 34(01): 61–64.

Liang, F., Gao, L., Wang, Z.H., Wang, T., and Liu, K., 2018. A pilot project of ambient noise tomography on a dense seismic array in Ji'nan urban area*. Earthquake Science, 31: 262–271.

Liang, F., Gao, L., Wang, Z.H., Li, H.L., Liu, K., Wang, T., and Li, X.Z., 2019a, Study of the shear wave velocity structure of underground shallow layer of Jinan by ambient noise tomography. Earth Science Frontiers, 26(3): 129–139 (in Chinese with English abstract).

Liang, F., Wang, Z.H., Li, H.L., Liu, K., and Wang, T., 2019b, Near-surface structure of downtown Jinan, China: Application of ambient noise tomography with a dense seismic array. Journal of Environmental and Engineering Geophysics, 24 (04): 641–652.

Liu, C.M., Yao, H.J., Yang, H.Y., Shen, W.S., Fang, H.J., Hu, S.Q., and Qiao, L., 2019. Direct inversion for the three-dimensional shear wavespeed azimuthal anisotropy based on surface-wave ray tracing: Methodology and application to Yunnan, southwest China. Journal of Geophysical Research, 124(11): 11394–11413.

Liu, H.S., 2009. Surface exploration about the Qianfoshan Fault in Jinan city. Seismological Research of Northeast China, 25 (3): 59–65 (in Chinese with English abstract).

Liu, Q.H., Lu, L.Y., and Wang, K.M., 2015. Review on the active and passive surface wave exploration method for the near-surface structure. Progress in Geophysics, 30(6): 2906–2922.

Miao, Q.J., Liu, X.Q., Shi, Y.Y., Qu, J.H., Zheng, J.C., and Tian, F.D., 2009. Tectonic stress analysis based on the crustal seismic anisotropy in the Shandong area. Earthquake Research in China, 32(1): 63–71.

Qian, J.Z., Zhan, H.B., Wu, Y.F., Li, F.L., and Wang, J.Q., 2006. Fractured-karst spring-flow protections: A case study in Jinan, China. Hydrogeology Journal, 14: 1192–1205.

Shi, Z.M., Li, C.L., Cheng, X.M., Liu, Y.X., Zhong, X.Y., and Jiang, Y.M., 2005. Geological characteristics of the geothermal field to the north of Jinan city. Shandong Land and Resources, 21(11): 39–42 (in Chinese with English abstract).

Song, W.J., Chen, S.J., Ge, F.G., Wu, Z.Q., and Lv, C.S., 2016. The analysis of comprehensive geophysical detection and seismicity of fracture of Mount Qianfo. CT Theory and Applications, 25(5): 523–530.

Sui, H.B., Kang, F.X., Li, C.S., Han, J.J., and Xing, L.T., 2017. Relation between north Jinan geothermal water and Jian spring water revealed by hydrogeothermal characteristics. Carsologica Sinica, 36(01): 49–58.

Wang, J.L., Jin, M.G., Lu, G.P., Zhang, D.L., Kang, F.X., and Jia, B.J., 2016. Investigation of discharge-area groundwaters for recharge source characterization on different scales: The case of Jinan in northern China. Hydrogeology Journal, 24: 1723–1737.

Wang, X., Wu, C.J., Li, Y., Li, G., and Xie, S.B., 2018a. Hydrogeological characteristics of the fault base area of Jinan Qianfoshan Mountain. Ground Water, 40(2): 11–14.

Wang, X., Wu, C.J., Xie, S.B., Li, Y., Zheng, C.Z., and Zhou, Y.Y., 2018b. Study on water conductivity and permeability of Qianfoshan Fault and Wenhuaqiao Fault in Jinan city. Shandong Land and Resources, 34(4): 50–55 (in Chinese with English abstract).

Wang, Z.J., 2002. Seismic anisotropy in sedimentary rocks, part 2: Laboratory data. Geophysics, 67(5): 1423–1440.

Wu, Q., and Xu, H., 2005. A three-dimensional model and its potential application to spring protection. Environmental Geology, 48(4–5): 551–558.

Xu, W.L., Wang, D.Y., Wang, Q.H., Pei, F.P., and Lin, J.Q., 2004. $^{40}Ar/^{39}Ar$ dating of hornblende and biotite in a Mesozoic

intrusive complex from the North China Block: constraints on the time of lithospheric thinning. Geochemistry, 33(3): 221–231.

Xu, Y.G., Huang, X.L., Ma, J.L., Wang, Y.B., Iizuka, Y., Xu, J.F., Wang, Q., and Wu, X.Y., 2004. Crust-mantle interaction during the tectono-thermal reactivation of the North China Craton: Constraints from SHRIMP zircon U-Pb chronology and geochemistry of Mesozoic plutons from western Shandong. Contributions to Mineralogy and Petrology, 147 (6): 750–767.

Yang, C.H., Xu, W.L., Yang, D.B., Liu, C.C., Liu, X.M., and Hu, Z.C., 2005. Chronology of the Jinan gabbro in western Shandong: Evidence from LA-ICP-MS zircon U-Pb dating. Acta Geoscientica Sinica, 26(4): 321–325.

Yang, L.Z., Qu, W.L., Liu, C.H., Shang, H., and Qi, X.F., 2012. Analysis of suitability of the division of engineering geological condition and rail transit construction in the Jinan urban area. Journal of Water Resources and Water Engineering, 23(06): 120–123.

Yao, H.J., Zhang, C., Lei, T., and Liu, Q.Y., 2018. Linear array ambient noise adjoint tomography with phases and amplitude ratios for high resolution crustal structures: Methodology and application. Acta Geologica Sinica (English edition), 92(z1): 287.

Zhang, D.W., Shu, J.C., and Sun, J.P., 2017. Observed deformation characteristics of a deep excavation for the spring area in Jinan, China. Journal of Mountain Science, 14(3): 581–594.

Zhang, Y.Y., Yao, H.J., Yang, H.Y., Cai, H.T., Fang, H.J., Xu, J.J., Jin, X., Kuochen, H., Liang, W.T., and Chen, K.X., 2018. 3-D crustal shear-wave velocity structure of the Taiwan Strait and Fujian, SE China, revealed by ambient noise tomography. Journal of Geophysical Research, 123(9): 8016–8031.

Zhao, Y.X., Li, C.S., and Xing, L.T., 2009. Formation conditions of the geothermal field in northern Jinan. Journal of the University of Jinan (Natural Science), 23(04): 406–409.

About the first author

LEI Ting, male, born in 1995 in Nanchong City, Sichuan Province; received his Master's Degree from the University of Science and Technology of China; Ph.D. student at the Department of Earth Science, University of Toronto. He is mainly engaged in research on ambient noise tomography and full-waveform inversion. E-mail: kdlt@mail.ustc.edu.cn.

About the corresponding author

LIANG Feng, male, born in 1982 in Fuping County, Shanxi Province, China; Philosophiae Doctor (Ph.D.) in Geophysics (Seismic Imaging) from the Chinese Academy of Geological Sciences, Beijing, then worked at the Chinese Academy of Geological Sciences. His early work was mainly on seismic reflection data processing and analysis for lithospheric structure and he has background knowledge in resources. Research in the last five years has concentrated on the research of ambient noise seismic data. In addition, considerable emphasis has also been placed on elegant solutions regarding underground space distinguishability and deep resource exploration. At the same time, as President of YES (Young Earth Scientists Network) China, he has been launching social academic activities for solving some common and livelihood issues related to earth science (http://yes-china.org.cn/), in order to create and build a whole chain of government, industry, education, research and application systems for young people in the field of earth science. E-mail: imr_liangfeng@cags.ac.cn; liangfeng@yes-china.org.cn.